Hypersonic Plasma Plume Expansion in Space

IEPC-2011-086

Presented at the 32nd International Electric Propulsion Conference, Wiesbaden, Germany September 11–15, 2011

Mario Merino*, Eduardo Ahedo†, Claudio Bombardelli‡, Hodei Urrutxua§ and Jesús Peláez¶
Universidad Politécnica de Madrid, 28040 Madrid (Spain)

Two-fluid analytical models of hypersonic plasma plumes, which are of great relevance in many applications, including a recently presented space debris deorbiting system based on plasma beams known as Ion Beam Shepherd, are discussed. A generalized framework to derive self-similar models is provided, from which three particular models proposed in the literature are derived and compared. It is demonstrated that strict self-similarity is incompatible with the two-fluid model. The three existing models provide only quasi self-similar solutions, based on a constant axial velocity and the order of the error is one over the square Mach number. A preliminary analysis of the effects of the ambient magnetic field on the plume is carried out, pointing out that resistivity, plasma-induced fields and the 3D geometry of the plasma provide three mechanisms that counter magnetic deflection of the plume.

I. Introduction

Hypersonic plasma plumes expanding in vacuum are ubiquitous in space electric propulsion: plasma thrusters of every type produce high-velocity plasma beams of different characteristics during operation.[1] In the space environment, plasma plumes are also created by plasma contactors,[2] used to control the electric charge of a spacecraft and to emit electrons from electrodynamic tethers to the surroundings. Plasma plumes of different sorts (e.g. created by pulsed laser ablation) are also important in industrial processes.[3]

Quick analysis and characterization of the plasma plume is paramount in preliminary design cycles of multiple applications, such as optimizing thruster orientation in the spacecraft to avoid plasma impingement on solar panels in geostationary satellites and other satellite parts,[4] identifying the relevant thruster parameters that dictate the beam divergence, or understanding plasma-surface interaction and deposition in industrial applications.[3] In these tasks, a fast and simple plasma model which is able to provide enough accuracy and detail of the different physical processes becomes a valuable tool. There exists an ample variety of models ranging in complexity and precision, from single-fluid, conical expansions[5] that yield rough analytical approximations to fully numerical particle models[6,7] that can reproduce detailed physics. In between, there exist a family of models[8–10] which depart from the same initial two-fluid equations, in which analytical solutions are achieved through claimed self-similarity. These so-called self-similar models (SSM) constitute an adequate trade-off between complexity and accuracy, and show good agreement with experimental results of both ion and Hall effect thrusters.[1,11,12]

An innovative application of plasma plumes of particular interest which has motivated the present work can be found in a space debris removal system which has been recently presented by our group.[13–16] Space debris constitute one of the main threats for continued commercial and scientific exploitation of space.[17] In the aforementioned removal concept, large pieces of space debris are deorbited using a plasma beam mounted on board of a controller spacecraft, known as Ion Beam Shepherd (IBS) and sketched in Fig.1.

*Student, mario.merino@upm.es (web.fmetsia.upm.es/ep2)
†Professor, eduardo.ahedo@upm.es
‡Researcher, claudio.bombardelli@upm.es
§Student, hodei.urrutxua@upm.es
¶Professor, j.pelaez@upm.es

The plasma plume from an electric thruster is directed towards the target debris to exert a continuous deorbiting force, which under nominal operation is close to the thrust produced by the thruster. In this way, the technologically-challenging docking maneuver with an uncooperative, tumbling object is avoided. The IBS is equipped with a second propulsion system that counters the thrust produced upon it by the plasma beam. As the IBS transmits momentum to the debris, it accompanies it during the deorbiting operation while maintaining close formation flying, until delivering it to the desired reentry orbit (or to a disposal orbit). The SSM models object of this paper are being used in the study of the IBS system.

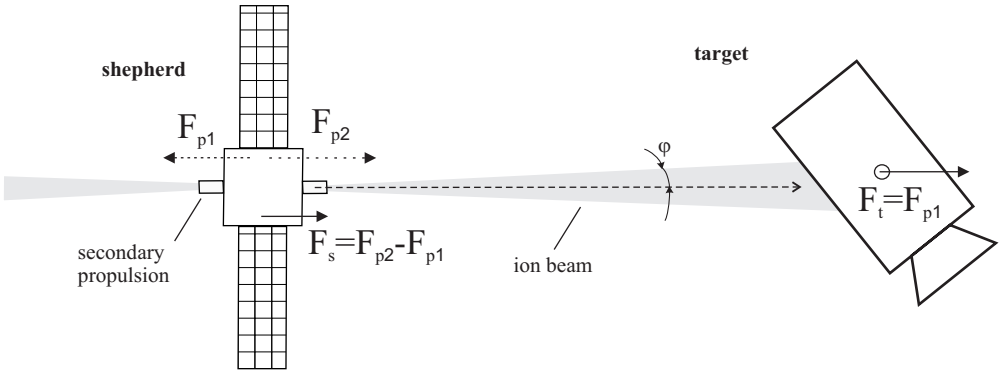

Figure 1. Schematic of ion beam shepherd satellite deorbiting a space debris

The main goal of this paper is to provide a generalization of SSM of plasma plume expansion in vacuum, by establishing a single two-fluid model framework and its solutions based on variable separation. This framework, which can also be used as the starting point for the derivation of other SSM, is presented in section II. We demonstrate that rigorous self-similar solutions of the two-fluid model do not exist unless the ion axial momentum equation is simplified for hypersonic flows. The local error in this equation is measured. We focus our attention in a subset of SSM which assumes constant axial velocity along ion streamlines. The three individual models of Parks and Katz,[8] Ashkenazy and Fruchtman[9] and Korsun and Tverdokhlebova,[10] which all belong to this group, are then particularized from the general equations and discussed in detail in subsections A and B, showing that actually none of them is strictly self-similar.

The rest of this work is devoted to the analysis of the influence of external magnetic fields on the development of the plasma plume. Magnetic fields, if strong enough, might deflect the plasma beam. The inclusion of these effects breaks the quasi-self-similarity of the hypersonic plume, and the analysis of the resulting problem becomes a complex 3D problem since different phenomena need to be taken into account simultaneously, including (1) the effects of cross-field diffusion via resistivity, (2) the role of the induced magnetic field, and (3) the finite width of the plasma beam. A preliminary study of these effects is carried out in section III, based on the solution of the unperturbed plasma plume from SSM.

Finally, section IV summarizes the main points of this work.

II. Expansion of a hypersonic plasma plume in vacuum

As the high-velocity plasma abandons the thruster chamber, a plasma plume forms and expands into space. The plume can be divided in two regions. First, close to the thruster, plasma inhomogeneities and thruster electromagnetic fields dominate the expansion. In the case of gridded ion thrusters, the beam is initially formed by numerous beamlets, produced by each aperture in the grids, which soon coalesce into a single-peaked plasma profile, typically in a distance less than a thruster radius.[18] The grids and the neutralizer electric fields influence the initial stages of expansion. Hall thrusters, on the other hand, produce an initially annular beam, with strong magnetic fields still present after the thruster exit section. These fields play a role in the final ion acceleration stages. The plasma profile becomes single-peaked after about 2 thruster radii away from the exit plane.[19] In this region, which can be termed *near-field*,[20] plasma modeling is a complex task, and usually full numerical models are required for its study. The initial divergence angle of the beam results from the processes taking place in this region.

After this initial expansion region, a smooth, bell-shaped plasma profile is established. Thruster fields and most plasma interactions become negligible: the plasma plume continues to expand under the action

of its residual pressure and the internal ambipolar electric fields, forming a proper plasma plume. This *far-field*[21] region is relevant to various plasma applications, and is susceptible of being described with simplified models, such as the SSM derived below. In the following, we derive the general SSM equations for a plasma plume starting from the fluid equations of ions and electrons.

The steady-state, axisymmetric, quasineutral plasma plume is assumed non-collisional, non-rotating, globally current-free, and formed by single-charged cold ions (i) and hot electrons (e). Here, we assume that it expands into vacuum with no ambient magnetic field. A cylindrical coordinate system (z, r, θ), with z along the plume axis and the origin placed on the plume centerline at an arbitrary initial plane in the far-field, will be used for the description of the plasma plume.

Under the aforementioned assumptions, the following fluid equations govern the plasma:

$$u_{zi}\frac{\partial \ln n}{\partial z} + u_{ri}\frac{\partial \ln n}{\partial r} + \frac{\partial u_{zi}}{\partial z} + \frac{1}{r}\frac{\partial (r u_{ri})}{\partial r} = 0, \tag{1}$$

$$u_{zi}\frac{\partial u_{zi}}{\partial z} + u_{ri}\frac{\partial u_{zi}}{\partial r} + \frac{e}{m_i}\frac{\partial \phi}{\partial z} = 0, \tag{2}$$

$$u_{zi}\frac{\partial u_{ri}}{\partial z} + u_{ri}\frac{\partial u_{ri}}{\partial r} + \frac{e}{m_i}\frac{\partial \phi}{\partial r} = 0, \tag{3}$$

$$\frac{1}{n}\nabla n T_e - e\nabla\phi = 0, \tag{4}$$

where n, u_{zi}, u_{ri} are the plasma density and the ion velocity components in the z, r direction, ϕ the electric potential, and nT_e the electron pressure. In the electron momentum equation (Eq. 4), electron inertia has been neglected.

These equations need to be complemented with an equation of state for electrons. We will assume a polytropic relation:

$$p_e = p_e(n) = p_{e0}\frac{n^\gamma}{n_0^\gamma}, \tag{5}$$

where γ is the effective specific heat ratio of electrons and the subindex 0 denotes variables at the origin. According to experimental results,[22] γ is close to 1, meaning that electrons evolve almost isothermally along the plume, $T_e = \text{const}$. This results from the large electron thermal conductivity in the plume, which tends to homogenize the temperature everywhere. For $\gamma > 1$ the electron momentum equation (Eq. 4) can be rewritten as:

$$\frac{\gamma}{\gamma - 1}\frac{T_{e0}}{n_0^{\gamma-1}}\nabla n^{\gamma-1} - e\nabla\phi = 0. \tag{6}$$

The isothermal limit corresponds formally to $\gamma \to 1$, for which Eq. 4 results in $T_{e0}\nabla \ln n - e\nabla\phi = 0$.

All these equations can be normalized using T_{e0} (electron temperature at the chosen origin), m_i (ion mass), e (elementary electric charge), n_0 (particle density at the origin), and the characteristic length R_0, which will be defined as the radius of the plasma tube at $z = 0$ containing a specified fraction of the total ion flux of the plume (in particular, the tube containing 95% of the flow, since this tube is used conventionally to define the plume divergence angle). In the following, dimensionless variables will be denoted with a hat, e.g., $\hat{\phi} = e\phi/T_e$, $\hat{u}_{zi} = u_{zi}/\sqrt{T_{e0}/m_i}$.

These equations constitute the starting point for the variable-separation SSM considered here. These SSM are based in two fundamental assumptions: first, that all ion streamlines $r_i(z_i)$ expand likewise, so they can be expressed through a dimensionless self-similarity function $h(\hat{z})$,

$$\hat{r}_i(\hat{z}_i) = \hat{r}_{i0} h(\hat{z}_i), \tag{7}$$

where r_{i0} is the radius of the streamline at $\hat{z} = 0$, and $h(0) = 1$. It follows that ion velocity components are related by the expression

$$\hat{u}_{ri} = \hat{r}\frac{h'}{h}\hat{u}_{zi}. \tag{8}$$

Second, it is assumed that flow variables $\hat{u}_{zi}$ and $\hat{n}$ can be separated as

$$\begin{aligned} \hat{u}_{zi}(\zeta, \eta) &= u_c(\zeta)\, u_t(\eta), \\ \hat{n}(\zeta, \eta) &= n_c(\zeta)\, n_t(\eta), \end{aligned} \tag{9}$$

where ζ and η constitute a new coordinate system, with

$$\zeta = \hat{z}, \quad \eta = \frac{\hat{r}}{h\left(\hat{z}\right)}. \tag{10}$$

This separates the axial evolution of the variables at the centerline (functions with subindex c) and their radial profiles (subindex t). On the z-axis, $u_t\left(0\right) = n_t\left(0\right) = 1$. Notice that $u_c\left(0\right) = \sqrt{\gamma}M_0$, with $M_0 = u_{zi}\left(0,0\right)/\sqrt{\gamma T_{e0}/m_i}$ the Mach number at the origin.

Introducing this solution in the continuity equation (eq. 1) yields:

$$h^2 n_c u_c = \sqrt{\gamma}M_0, \tag{11}$$

Similarly, momentum equations 2 and 3 reduce to:

$$u_c u_c' u_t^2 + \gamma\left(n_c n_t\right)^{\gamma-2}\left(n_c' n_t - n_c n_t' \eta\frac{h'}{h}\right) = 0, \tag{12}$$

$$\frac{h u_c\left(u_c h'\right)'}{n_c^{\gamma-1}} = -\frac{\gamma n_t^{\gamma-2} n_t'}{\eta u_t^2} = \gamma C, \tag{13}$$

where C is a separation constant.

The set of equations 11–13 is in general incompatible with the selfsimilarity assumption, eq. 7, and the solution structure imposed in Eq. 9. This is reflected by the fact that eq. 12 is not separable in the same fashion as 13: in fact, fulfillment of this equation can be subdivided into (1) satisfying it at the centerline,

$$u_c u_c' + \gamma n_c^{\gamma-2} n_c' = 0, \tag{14}$$

i.e., Bernoulli relation for the conservation of energy in this streamline,

$$\frac{u_c^2}{2} + \frac{\gamma}{\gamma-1}n_c^{\gamma-1} = \frac{\gamma M_0^2}{2} + \frac{\gamma}{\gamma-1},$$

($u_c^2/2 + \ln n_c = M_0^2/2$ for isothermal [$\gamma = 1$] flows); plus (2) the following conditions resulting from equating to zero the η-derivative of Eq. 12:

$$\frac{n_c'}{n_c}\frac{h}{h'} = -\frac{2n_t'}{2n_t u_t'/u_t - \left(\gamma-1\right)n_t'} = D, \tag{15}$$

i.e.,

$$n_c = h^D, \tag{16}$$

$$n_t^{2-D(\gamma-1)} = u_t^{-2D}, \tag{17}$$

with D another separation constant. Expressions 11, 13, 14 and 15 contain 6 equations for the 5 variables h, u_c, u_t, n_c and n_t, so the problem is over-determined. Indeed, rewriting Eq. 14 with the assistance of expressions 11 and 16,

$$\left[-\left(2+D\right)\gamma M_0^2 h^{-(5+2D)} + \gamma D h^{D(\gamma-1)-1}\right]h' = 0, \tag{18}$$

it turns apparent that to vanish the term in brackets requires $D = -4/\left(\gamma+1\right)$ and $M_0^2 = -2/\left(\gamma-1\right)$, which yields $M_0^2 < 0$ for $\gamma > 1$ (and $M_0^2 \to -\infty$ for $\gamma \to 1$). This nonphysical result manifests the nonexistence of rigorous self-similar solutions of this sort.

Therefore, any of these SSM of a plasma plume is only an approximation of the real flow. However, the advantages of having a simple, semi-analytical model encourage elaborating SMM further. To proceed with the derivation of an approximated SSM, it is unavoidable to free one of these constraints, or perform an adequate assumption about the variables.

It follows from Eq. 14 that when the flow is highly hypersonic $M_z \gg 1$, the axial velocity variations along streamlines are small compared to velocity itself: $\Delta M_z/M_z \sim \Delta \ln n/M_z^2 \ll 1$, where $M_z = u_{zi}/\sqrt{\gamma T_e/m_i}$ is the local axial Mach number of the flow. Taking advantage of this, a common approach of existing SSM

for hypersonic plasma plumes consists in substituting ion axial momentum Eq. 2 for an adequate expression for u_c and u_t instead. The relative local error $\varepsilon(\zeta,\eta)$ committed by this substitution can be evaluated with the dropped equation:

$$\begin{aligned}\varepsilon(\zeta,\eta) &= \frac{\hat{u}_{zi}\partial\hat{u}_{zi}/\partial\hat{z}+\hat{u}_{ri}\partial\hat{u}_{zi}/\partial\hat{r}+\gamma\hat{n}^{\gamma-2}\partial\hat{n}/\partial\hat{z}}{\hat{u}_{zi}^2} = \\ &= \frac{u_c'}{u_c}+\frac{\gamma(n_c n_t)^{\gamma-2}}{u_c^2u_t^2}\left(n_c'n_t-n_cn_t'\eta\frac{h'}{h}\right)=\frac{u_c'}{u_c}+\frac{1}{M_z^2}\left(\frac{n_c'}{n_c}-\eta\frac{h'}{h}\frac{n_t'}{n_t}\right),\end{aligned} \tag{19}$$

where the first part of the error in the right hand side is $(\ln u_c)'$, and the latter is $\propto 1/M_z^2$. Therefore, if $u_c=$ const is assumed, this error is arguably small for actual ion or Hall thruster plumes (for which $M_0>20$, see Ref. 23).

A. Family of models with $u_c=$ const

The most relevant family of SSM substitutes Eq. 2 with the condition $u_c=\sqrt{\gamma}M_0=$ const and an additional hypothesis for the u_t profile. As explained above, this is appropriate for hypersonic flows, since u_{zi} varies very little along the axis. The $u_c=$ const condition means that plasma axial velocity along streamlines is frozen, and hence the first part of the error in equation 19 vanishes.

Continuity Eq. 11 leads to

$$n_c=\frac{1}{h^2}. \tag{20}$$

Then, the first equation of expression 13 produces a ordinary differential equation for h:

$$h^{2\gamma-1}h''=\frac{C}{M_0^2}. \tag{21}$$

Integration of Eq. 21 yields

$$h'=\sqrt{\delta_0^2-\frac{C}{M_0^2(\gamma-1)}\left(h^{-2(\gamma-1)}-1\right)} \tag{22}$$

for polytropic $\gamma\neq 1$ flows and

$$h'=\sqrt{\delta_0^2+\frac{2C}{M_0^2}\ln h} \tag{23}$$

for isothermal $\gamma=1$ flows. In these expressions and below, $\delta_0=h'(0)$ is the tangent of the velocity at $\zeta=0$, $\eta=1$. Notice that this can be further integrated as $\int_1^h dh/h'=\zeta$, from where h is implicitly defined. In the polytropic case, $h'\to\sqrt{\delta_0^2+C/\left[M_0^2(\gamma-1)\right]}$ far downstream; for the isothermal case, $h'\to\infty$.

Equations 20 and 21 determine n_c and h. It only remains to set u_t and n_t. The second equation in expression 13 provides a relation between the two:

$$\ln n_t=-C\int_0^\eta \eta u_t^2 d\eta \tag{24}$$

for isothermal $\gamma=1$ flows and

$$n_t^{\gamma-1}=1-(\gamma-1)C\int_0^\eta \eta u_t^2 d\eta \tag{25}$$

for polytropic flows. This expression reveals the existence of a $\eta_{max}\in[0,\infty[$ beyond which $n_t=0$ for polytropic flows, whereas $\eta_{max}=\infty$ in an isothermal plasma. The local error ε committed can be expressed as:

$$\varepsilon=\frac{C}{M_0^2}\frac{h'}{h^{2\gamma-1}}\eta\left(2\frac{n_t}{n_t'}+\eta\right). \tag{26}$$

This expression reveals that the error is proportional to $h''h'$, and points out that to completely vanish the local error, the density profile should satisfy $n_t' = -2/\eta^3$. However, this represents an unpractical case with density becoming singular at $\eta = 0$. There is nevertheless a streamline $\eta^* = -2n_t/n_t'$ for which the local error is zero.

Particular models can now be derived choosing a profile for u_t, which then determines n_t. From among the models of this family, (1) the Parks and Katz model (PK),[1,8] (2) the Ashkenazy and Fruchtman model (AF),[9] and (3) the Korsun and Tverdokhlebova model (KT)[10] are reviewed below. The PK and AF models are generalized to the non-isothermal case.

The **PK model** takes $u_t = 1 = \text{const}$ which leads to:

$$n_t = \exp\left(-C\frac{\eta^2}{2}\right) \tag{27}$$

for isothermal flows ($\gamma = 1$) and

$$n_t = \left(1 - (\gamma - 1)\, C\frac{\eta^2}{2}\right)^{1/(\gamma-1)} \tag{28}$$

for polytropic flows. The local error ε and zero-error streamline η^* for this model can be reduced to:

$$\varepsilon = \frac{C}{M_0^2}\frac{h'}{h^{2\gamma-1}}\left(\eta^2 - \frac{2}{C}\right); \quad \eta^* = \sqrt{\frac{2}{C}}. \tag{29}$$

In the case of the isothermal flow, a practical choice of constant C can be made to have the ion flux inside the $r \leq R_0$ tube, $G_i\,(\eta = 1)$, equal to 95% of the total beam flux. Integrating over the initial plane, one has

$$\frac{G_i\,(\eta = 1)}{G_i\,(\eta_{max} = \infty)} = 1 - e^{-C/2} = 0.95 \Rightarrow C = -2\ln 0.05 \simeq 6. \tag{30}$$

In the polytropic case C can be calculated likewise, with $\eta_{max} = \sqrt{2/\left[(\gamma - 1)\, C\right]}$ the last plasma streamline.

The **AF model**, on the other hand, employs a conical velocity profile at the initial plane, $\zeta = 0$, so that u_t is given by

$$u_t = \frac{1}{\sqrt{1 + \eta^2/\hat{d}^2}}, \tag{31}$$

with $\hat{d}$ a parameter that represents the dimensionless distance from the cone vertex used to define the flow to the initial plane, which is related to the velocity tangent at $\zeta = 0$, $\eta = 1$ as $\hat{d} = \delta_0^{-1}$. Expression 31 for u_t produces the following profile n_t:

$$n_t = \frac{1}{\left[1 + \eta^2/\hat{d}^2\right]^{C\hat{d}^2/2}}; \quad \varepsilon = \frac{C}{M_0^2}\frac{h'}{h}\left(\eta^2 - 2\frac{1 + \eta^2/\hat{d}^2}{C}\right); \quad \eta^* = \left(\frac{C}{2} - \frac{1}{\hat{d}^2}\right)^{-1/2}, \tag{32}$$

for isothermal flows. Here, it is seen that error dependence with η disappears when $\hat{d}^2 = 2/C$. For this case, η^* is not defined. For the polytropic flow, one has:

$$n_t = \left[1 - \frac{C\hat{d}^2(\gamma - 1)\ln\left(1 + \eta^2/\hat{d}^2\right)}{2}\right]^{1/(\gamma-1)}, \tag{33}$$

$$\varepsilon = \frac{C}{M_0^2}\frac{h'}{h^{2\gamma-1}}\left[\eta^2 - 2\frac{1 + \eta^2/\hat{d}^2}{C} + (\gamma - 1)\left(\hat{d}^2 + \eta^2\right)\ln\left(1 + \frac{\eta^2}{\hat{d}^2}\right)\right], \tag{34}$$

and, the zero-error streamline η^* can be determined numerically equating to zero Eq. 34. Again, constant C can be set to locate the 95% flux tube at $\eta = 1$. For the isothermal case one has:

$$\frac{G_i\,(\eta = 1)}{G_i\,(\eta_{max} = \infty)} = 1 - \left(1 + \frac{1}{\hat{d}^2}\right)^{\left(1 - C\hat{d}^2\right)/2} = 0.95. \tag{35}$$

Finally, the **KT model** is based on the fulfillment of condition 17, resulting in the following profiles for n_t and u_t. The separation constant D in Eq. 16 is chosen $D = -2$, in agreement with continuity Eq. 11:

$$n_t = \left(1 + C\frac{\eta^2}{2}\right)^{-1}, \tag{36}$$

$$u_t = \left(1 + C\frac{\eta^2}{2}\right)^{-\gamma/2}. \tag{37}$$

The value of C this time is given by:

$$\frac{G_i\left(\eta = 1\right)}{G_i\left(\eta_{max} = \infty\right)} = 1 - \left(1 + \frac{C}{2}\right)^{-\gamma/2} = 0.95, \tag{38}$$

for both the isothermal and polytropic cases. The local error is now independent of η:

$$\varepsilon = \frac{-2}{M_0^2}\frac{h'}{h^{2\gamma-1}}, \tag{39}$$

so that there is no zero-error streamline η^* in this case. This model coincides with the AF model when $\hat{d}^2 = 2/C = \delta_0^{-2}$ in the isothermal case. It is noted here that Korsun and Tverdokhlebova[10] also present a variant of their model in which u_c is not constant. However, in that case, the first term of the ε error in Eq. 19, which is not proportional to $1/M_0^2$, is not zero. Here, we have chosen to limit our attention to the constant u_c case, for which that error term is null.

As a final note to conclude this section, other models of this type can be derived by simply imposing the desired profile for u_t or n_t and calculating the other variables from it. The error ε can be used to measure the quality of the model.

B. Discussion of the three models

This section compares the three models in the isothermal case. The models developed in the previous section depend on two parameters, M_0 and δ_0, that reflect the influence of the thruster and the phenomena taking place in the near-field. These parameters control the shape of the h function that defines the streamlines of the flow, as depicted in Fig. 2. As it can be seen, the Mach number plays an important role in the divergence increase rate of the plume. Actually, M_0^2 is basically the thermal-to-kinetic energy ratio of the beam,

$$M_0^2 \sim \frac{m_i u_i^2}{T_e}, \tag{40}$$

and hence dictates the radial expansion of the plasma. Clearly, the plume is not conical, although for sufficiently small distances, its shape can be adequately approximated by a cone. From Eq. 23 for an isothermal plasma, it can be said that the plume around position $\zeta = \zeta_*$ departs little from a cone while $\ln\left(h/h_*\right) \ll M_0^2\delta_*^2/\left(2C\right)$. Hence, $h \simeq h_* + \delta_*\left(\zeta - \zeta_*\right)$ up to distances of the order $\zeta - \zeta_* \sim \Delta\zeta_{crit}$:

$$\Delta\zeta_{crit} = \frac{\exp\left(M_0^2\delta_*^2/\left(2C\right)\right) - 1}{\delta_*}h_*,$$

which increases with M_0, δ_* and h_*. This shows that plume curvature decreases as it expands, since the conical approximation is better suited the larger ζ_* is.

The profiles for $\hat{n}$, $\hat{n}\hat{u}_{zi}$, and $\hat{n}\hat{u}_{ri}$ for the three models derived in the previous section are plotted in figures 3, 4 and 5 for a representative isothermal plasma ($M_0 = 20$ and $\delta_0 = 0.2$). It is seen that both PK and AF models yield very similar profiles. A stronger difference is observed with respect to the KT model where the $\eta = 1$ streamline diverges much faster. The reason for this resides in the different plasma axial fluxes $\hat{n}\hat{u}_{zi}$ produced by each model as explained below, and the condition of 95% flux at $\eta = 1$ used to calculate C produce a plasma density profile that decays much more rapidly in the radial direction than in the other models.

One of the key differences between the models is their axial flux profile $n_t u_t$. This is more easily studied in sight of the flux integrals for the three models of Fig. 6. For instance, in the isothermal PK model, flux decreases exponentially with η. In contrast, KT flux decreases algebraically with η, producing a flux profile

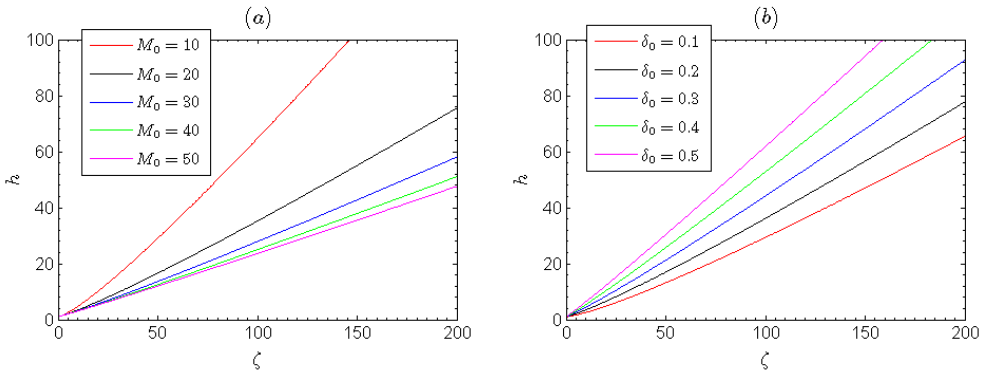

Figure 2. Shape of the plume streamlines (h function) for different values of the Mach number M_0 and the initial divergence angle δ_0. In Fig. (a), $\delta_0 = 0.2$, and in Fig. (b), $M_0 = 20$.

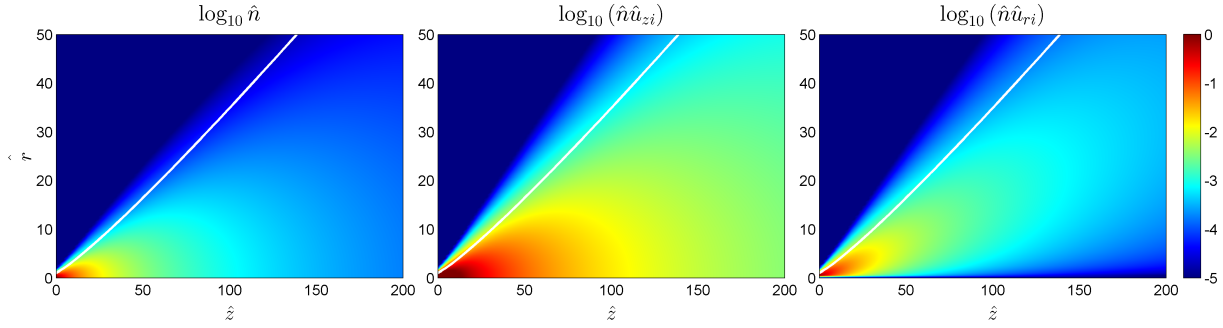

Figure 3. Results for PK model with isothermal electrons ($\gamma = 1$) and $\delta_0 = 0.2$, $M_0 = 20$. Logarithm scale has been used for the plots. The white line in each graph denotes the $\eta = 1$ streamline, dictated by the h function.

with thicker peripheral plasma, giving rise to the large differences in the figures with respect to the other models. Interestingly, the AF model coincides with PK for $\hat{d} \to \infty$, since

$$n_t u_t|_{AF} = \left(1 + \frac{\eta^2}{\hat{d}^2}\right)^{(C\hat{d}^2+1)/2} \underset{(\hat{d}\to\infty)}{\longrightarrow} \exp\left(\frac{C\eta^2}{2}\right) = n_t u_t|_{PK} \,,$$

(although for finite $\hat{d}$, the dependency with η is always algebraic); and on the other hand, it coincides with KT when $\hat{d}^2 = 2/C = \delta_0^{-2}$ ($\hat{d} \simeq 0.05$), and the flux also exhibits a slow decrease with η [for the presented case with $\hat{d}^{-1} = \delta_0 = 0.2$, $\hat{d}$ is large and AF model closely resembles PK in Fig. 6].

When calculating C with a condition like Eq. 30, we are radially contracting the plasma solution to fit 95% of the total flux in the $\eta = 1$ streamtube. The large value of C required for this in the models with more dense peripheral plasma implies a fast increase of the divergence angle, and strongly-peaked plasma profiles at the origin. Hence, in order to have a more convenient plasma profile with KT and large-δ_0 AF, it is suggested to use an alternative condition to define C, such as a given n/n_0 fraction at $\eta = 1$ (with the inconvenience of having a significant fraction of the plasma flux at large η, which might be undesired for some applications).

The relative local error ε of each model is presented in Fig. 7. The error of PK is small and displays a zero-error streamline. The quality of the solution deteriorates for large η. This is not an issue for most applications concerned with plasma momentum flux, as the momentum transported by the plasma far from the centerline is negligible. However, it can be a problem when the variable of interest is the plasma density or the local velocity components of ions in that region. The error is η-independent for the KT model (and the AF model when it coincides with it), showing that this model can have advantages for applications where plasma density outside of the bulk of the plume is important. As discussed above, AF model behaves similarly to PK for small values of δ_0, although it approaches the behavior of KT model for larger δ_0.

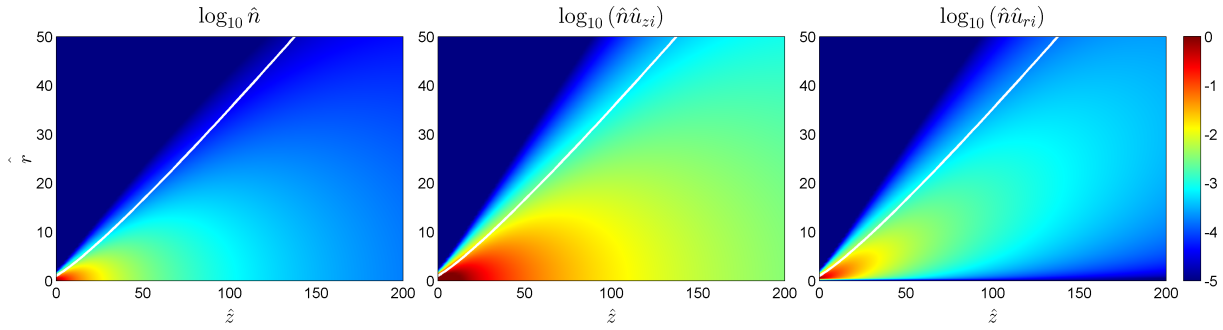

Figure 4. Results for AF model with isothermal electrons ($\gamma = 1$), $\delta_0 = 0.2 = \hat{d}^{-1}$ and $M_0 = 20$.

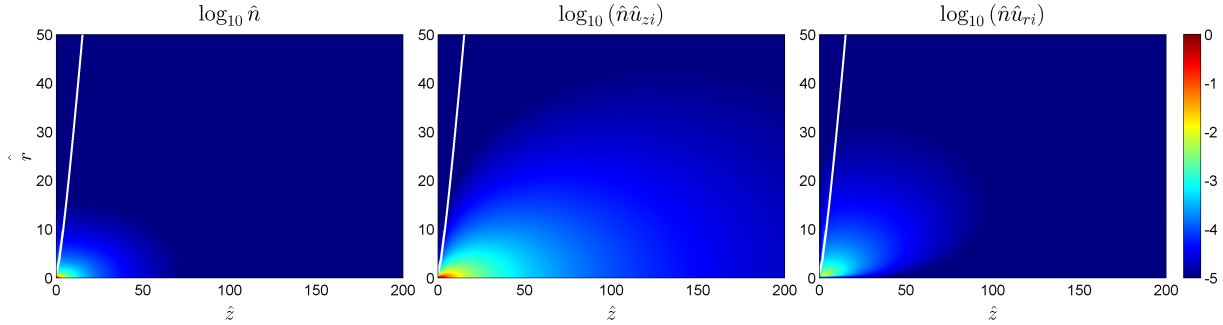

Figure 5. Results for KT model with same conditions as Fig. 3 and 4.

III. Influence of external magnetic fields

The plasma expansion studied in section II can be altered by the environment. In particular, two phenomena influence the development of the plume: (1) collisions with ambient plasma, and (2) the presence of an external magnetic field.

Needless to say, the inclusion of any extraneous effects such as these breaks the quasi-selfsimilarity of the model. Accurate simulation of collisional and magnetic effects requires the use of full numerical models, which lack the advantages in terms of speed and simplicity of a SSM. In this section, a preliminary assessment of the influence of these effects is carried out based on the solution obtained for the plasma plume expansion in vacuum.

The plasma plume loses momentum to the environment through collisional processes with background particles. As a result, the plume is progressively decelerated (eventually, until both plume and background velocities coincide), and the divergence rate of the beam is increased. Collisions with the stationary ambient ($u_{za} \ll u_{zi}$, with u_{za} the mean velocity of ambient particles) can be evaluated from the ion axial momentum equation

$$u_{zi}\frac{\partial u_{zi}}{\partial z} + u_{ri}\frac{\partial u_{zi}}{\partial r} + \frac{e}{m_i}\frac{\partial \phi}{\partial z} = -\nu_{ia}u_{zi}, \tag{41}$$

where ν_{ia} is the effective collision frequency of ions with the ambient particles. From here, it is seen that as long as $\nu_{ia}LM_0/\sqrt{T_e/m_i} \ll 1$, collisional effects over distances in the order of L can be neglected. In practical electric propulsion systems in space (ambient density $n_a \simeq 10^{10}\,\mathrm{m}^{-3}$ in low Earth orbit), $L \sim 1$ km or larger, and therefore ambient particles exert a negligible effect. This might not be the case for industrial and vacuum chamber testing applications, where the vacuum quality might be low.

Magnetic fields can cause the deflection of the plasma plume, which tends to align with the direction of $\boldsymbol{B}$, breaking the existing axisymmetry. They can also channel the plume and limit its expansion, in a somehow similar fashion to a magnetic nozzle.[24] In order to take place, magnetic deflection of the plume requires the existence of a plasma current density, $\boldsymbol{j} = en\,(\boldsymbol{u}_i - \boldsymbol{u}_e)$, so that a force density $\boldsymbol{j} \times \boldsymbol{B}$ is generated on the

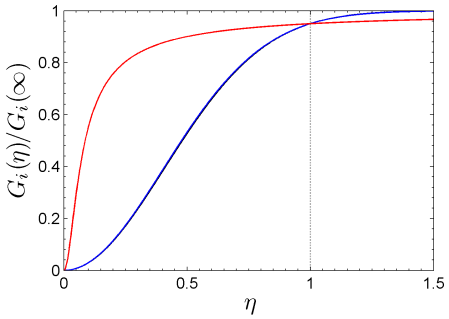

Figure 6. Integrated ion flux $G_i(\eta) = \int_0^\eta 2\pi\eta\hat{n}\hat{u}_{zi}d\eta$ in the isothermal case, normalized with $G_i(\eta_{max} = \infty)$, for the three models (PK black, AF blue, KT red; the black and blue lines are indistinguishable at the scale used). A representative initial divergence $\delta_0 = 0.2$ has been chosen for these images. The condition of 95% flux at $\eta = 1$ has been imposed for all models. The black (PK model) and blue (AF model) lines are very close to each other for low values of δ_0. The flux of PK and KT models is independent of δ_0, but it is not so for AF: as δ_0 increases, AF separates from PK and approaches KT (red line), perfectly coinciding with it when $\hat{d}^2 = 2/C = \delta_0^{-2}$.

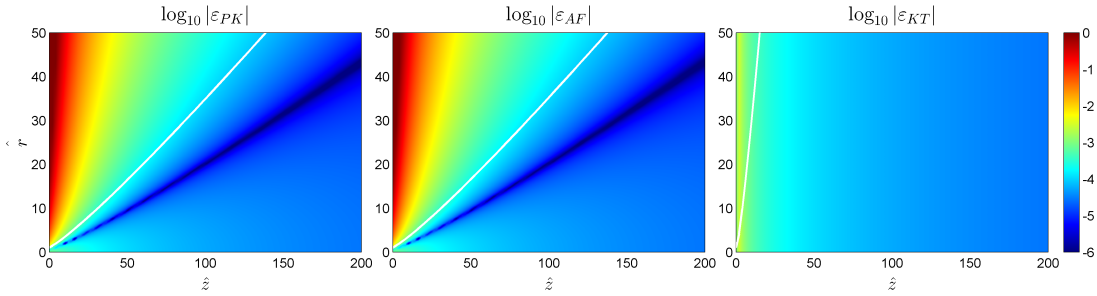

Figure 7. Relative local error ε of each isothermal model as defined in Eq. 19.

plasma. In the presence of a homogeneous external magnetic field $\boldsymbol{B}$, plasma currents parallel to $\boldsymbol{u}_i \times \boldsymbol{B}$ can be induced as the positive and negative charges react differently to the field. These currents then interact with $\boldsymbol{B}$ and can lead to a net force in the direction $(\boldsymbol{u}_i \times \boldsymbol{B}) \times \boldsymbol{B}$ that acts on the plume and tends to bend it until $\boldsymbol{u}_i \parallel \boldsymbol{B}$.

If magnetic deflection occurs, it is important to assess over what distances the plume can be considered straight for practical purposes, and what plasma parameters govern the interaction. This is of particular interest in the plasma plume of the IBS concept described in the Introduction, where the goal is to direct the plasma against a target space debris, and a safe distance to the object must be kept. Similarly, in vacuum chamber testing of plasma thrusters, magnetic effects can be responsible of a non-negligible beam deflection and hence a perturbation of the measurements if not compensated (see for example Ref. 25).

For propulsive applications, it is interesting to note that the reaction force to this deflection will be felt by the generator of the external field $\boldsymbol{B}$, transmitted via the induced magnetic field that the plasma currents create. Hence, if the magnetic field has its origin in the spacecraft, the latter will suffer a secular torque. [In the case of the geomagnetic field, the reaction is exerted on the Earth itself].

Based on their self-similar solution, Korsun and Tverdokhlebova predict a very strong deflection of keV ion beams in low Earth orbit ($B \simeq 0.5$ G) in less than one meter.[26] However, a precise evaluation of magnetic effects requires a complete numerical model, as the introduction of a magnetic field brings about additional phenomena related to (1) plasma resistivity, (2) plasma induced magnetic fields and (3) the finite width of the plume, which are paramount to evaluate the plasma response. We are uncertain whether in their analysis, Korsun and Tverdokhlebova consider or ignore the two last effects. More importantly this plethora of effects and mechanisms destroys the axisymmetry and self-similarity of the plume, indicating that an analysis based on SSM is not feasible.

Indeed, a SSM might be used to provide only a rough estimation in the case where the magnetic field is coaxial with the original plume, since in this case axisymmetry is preserved. The effect of the magnetic

force in this scenario is to impede or confine the radial expansion of the plume. Two phenomena arise that compete with this confining effect: (1) diffusion thanks to resistivity, and (2) plasma-induced magnetic fields that oppose the external one and weaken $\boldsymbol{B}$. In absence of these two effects, confinement would be perfect, with charged particles departing from their magnetic line only distances of the order of their Larmor radius. In the following, we assess each effect separately.

To assess the importance of cross-field diffusivity due to collisions in the coaxial case we may study the first-order effects of including a small B_z, assuming that the expansion in the longitudinal plane is basically unperturbed. The magnetic field causes an electron azimuthal velocity component to appear as the plasma tries to expand across the field. This can be seen in the equation of motion of electrons in the θ direction, which after neglecting inertia reads:

$$eu_{re}B_z - \nu_{ei}m_e u_{\theta e} = 0 \Rightarrow u_{\theta e} = \chi_H u_{re}, \tag{42}$$

where ν_{ei} is the electron-ion collision frequency, m_e the electron mass, and $\chi_H = eB_z/(m_e\nu_{ei})$ the Hall parameter of the plasma. Similarly, ions will acquire a certain rotation, although their larger inertia assures that it will be negligible compared to electrons'. Hence, an azimuthal current density $j_\theta \simeq -en\chi_H u_{re}$ forms, which becomes stronger the lesser resistivity and the stronger B_z are. Then, neglecting ion rotation and longitudinal-plane collisions, this j_θ generates a Lorentz force in the plasma momentum equation in the r direction,

$$m_i\left(u_{zi}\frac{\partial u_{ri}}{\partial z} + u_{ri}\frac{\partial u_{ri}}{\partial r}\right) = -T_e\frac{\partial \ln n}{\partial r} - eB_z\chi_H u_{re}, \tag{43}$$

which tries to minimize radial expansion of the beam. Figure 8 shows the evolution of selected ion streamlines in an idealized plasma with $T_e \to 0$ immersed in a coaxial magnetic field. It is seen that in this case a magnetic field can be regarded as positive for certain applications such as the IBS, as the divergence of the plume can be reduced, and therefore the plasma can be channeled.

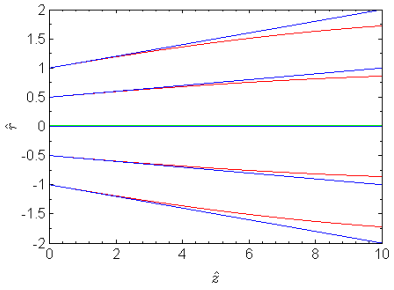

Figure 8. Development of ion streamlines under the effects of a coaxial magnetic field (directed along the green line). The plasma is assumed to have negligible thermal pressure ($T_e = 0$). A divergence $\delta_0 = 0.1$, Hall parameter $\chi_H = 20$ and ion gyroradius defined with the flow velocity $\ell_i = m_i u_{zi}/(eB_z) = 1000$ m are used, which are representative of a plasma plume from an ion thruster in low Earth orbit. Blue lines show ion streamlines in the absence of any magnetic field (conical expansion, since plasma has no pressure). The plasma suffers a confinement effect due to the presence of the magnetic field (red lines).

Comparing magnetic to inertial effects, the characteristic distance the plasma needs to travel to suffer noticeable channeling when taking into account collisional effects is

$$L_m \sim \frac{\ell_i}{\chi_H}, \tag{44}$$

where $\ell_i = m_i u_{zi}/(eB_z)$ is the ion Larmor radius based on the axial velocity u_{zi}. For a representative low Earth orbit case (800 Km altitude), where B is typically less than 0.5 G, a xenon plasma with $T_e = 2$ eV, $n_0 = 2.6\cdot10^{16}$ m^{-3}, and $M_0 = 20$, has $\nu_{ei} \simeq 3.17\cdot10^5$ s^{-1}, $\ell_i \simeq 1$ km, and $\chi_H \simeq 69.34$ (this large value of the Hall parameter does not account for turbulent effects, which might increase the effective collision frequency). Hence, $L_m \sim 14.4$ m. As mentioned already, the plasma is almost collisionless, and thus resistivity diffusion across $\boldsymbol{B}$ is expected to be small unless B is very weak. Indeed, in actual electric propulsion applications, $\chi_H \gg 1$, meaning low diffusion. This suggests that other effects such as the induced magnetic field can play

a more important role than collisions, meaning that this value of L_m is conservative and in practice it will be larger when these additional effects are taken into account.

Precise calculation of induced field effects is not possible with the present SSM models. However, a first estimation of the induced magnetic field, $\boldsymbol{B}_i$, can be made from Ampère's equation below. Induced fields are stronger the larger the azimuthal currents are. Now, neglecting resistivity and assuming $j_\theta B_z \sim T_e \partial n/\partial r$ from the electron momentum equation,

$$\frac{\partial B_{ri}}{\partial z} - \frac{\partial B_{zi}}{\partial r} = \mu_0 j_\theta \Rightarrow \frac{B_{zi}}{B_z} \sim \mu_0 \frac{nT_e}{B_z^2} = \beta. \tag{45}$$

Hence, the higher the plasma beta β, the stronger the induced magnetic field. For the same plasma at low Earth orbit as before, $\beta \simeq 1.61$. This large value of β shows that the induced field can totally cancel out the external field in most of the plume as long as plasma density n is large enough. The induced field therefore reduces the confining effect of the external field in the bulk of the plume. The effect on the peripheral plasma is however much more difficult to predict.

The study of a general case, with $\boldsymbol{B}$ at an angle α from the beam centerline, cannot be performed in the same fashion as before, since axisymmetry breaks. However, it is interesting to observe that, for large α angles, the finite width of the plasma plume gives rise to a third phenomenon that severely limits the influence of the magnetic field.

In contrast to the coaxial case, where the induced currents were azimuthal and needed not leave the plasma volume, in a general case the $\boldsymbol{j} \parallel \boldsymbol{u}_i \times \boldsymbol{B}$ currents need to traverse the whole plasma plume and then continue into the ambient plasma. The currents required to deflect the beam are proportional to its kinetic energy, and inversely proportional to the curvature radius of the deflected trajectories and the intensity of the field. Provided that the background density is much lower than the beam density (typically several orders of magnitude), fulfillment of current continuity $\nabla \cdot \boldsymbol{j} = 0$ demands very large velocities outside of the plume. Therefore, electron inertial effects and collisions will strongly limit the value of the cross-beam $\boldsymbol{j}$ that can develop, and hence the magnitude of the magnetic force $\boldsymbol{j} \times \boldsymbol{B}$ that deflects the plume. The effect is difficult to assess from our simple axisymmetric model, requiring a more detailed analysis. Ideally, in the case of zero ambient density, a clean plasma edge, and $\alpha = 90$ deg, when the magnetic field tries to deflect ions and electrons in opposite directions a strong electric field $\boldsymbol{E} \simeq -\boldsymbol{u}_i \times \boldsymbol{B}$ would appear to avoid charge separation (Hall effect), and absolutely no currents would exist in the steady-state (see sketch in figure 9). The $\boldsymbol{E} \times \boldsymbol{B}$ drift would then allow the plasma to continue its movement completely unperturbed.

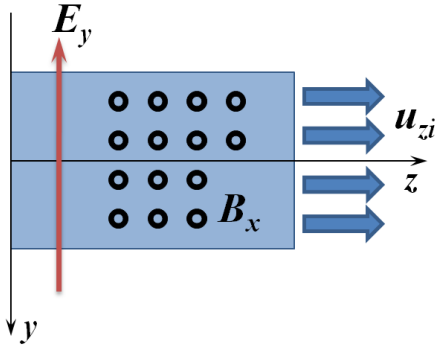

Figure 9. Sketch of an idealized, column plasma (with rectangular profile) with a clean boundary with vacuum. the plasma moves with a velocity $u_{zi} > 0$ at 90 deg with respect to the ambient magnetic field $B_x > 0$. To avoid charge separation, an electric field $E_y < 0$ forms (Hall effect), which then allows the plasma to continue its motion unaffected by B_x.

To sum up, this analysis suggests that magnetic effects will be weaker in low Earth orbit than previously expected,[26] especially for the large α case, as collisions and 3D geometry effects limit the development of the necessary currents, and the induced field competes with the external one.

IV. Conclusions

In this work we have presented a generalized model framework for two-fluid quasi-selfsimilar plume models. With it, three existing examples of SSM have been particularized and discussed. The framework

provides the necessary starting point to derive other models for general density profiles. The models serve as a fast and simple tool for the preliminary design of many plasma applications, including the novel active space debris removal concept known as "Ion Beam Shepherd".

We have demonstrated that no rigorous self-similar and separable solutions of the fluid equations exist. A measure of the error committed has been provided using the equation that the models fail to fulfill, and is shown to be proportional to the inverse of the square of the Mach number, $\propto 1/M^2$ (in the models of interest), and therefore they exhibit a high degree of accuracy in electric propulsion applications, where typically $M \gg 1$.

The roles of the governing parameters of the flow, the Mach number, and the initial divergence angle, have been quantified. It is seen that the Mach number has a strong influence on the rate at which the plume divergence angle increases. Profiles of the plasma variables and local error for a representative case of the three models have been calculated and compared. It is shown that two of the models are limit cases of the model of Ashkenazy and Fruchtman[9] for isothermal flows.

Additionally, a preliminary analysis of the influence of a homogeneous magnetic field on the development of the plume has been carried out, showing that magnetic fields can deflect the plasma beam and that (1) resistivity, (2) induced fields and (3) finite width of the plasma substantially reduce the effect of the external field on the plume, and that therefore they need to be retained in the analysis. The distances over which magnetic effects take place considering collisions has been roughly estimated from the plasma equations, and the importance of the induced fields assessed with the beta parameter.

Acknowledgements

The work for this paper was supported by the ARIADNA 'Call for Ideas on Active Debris Removal', established by the Advanced Concepts Team of the European Space Agency(ACT-ESA), under contract No. 4000101447/ 10/NL/CBi. Authors are very indebted to D. Petkow and L. Summerer of ACT-ESA for their useful comments. Additional support came from the Gobierno de España (Project AYA-2010-16699).

References

[1]Goebel, D. M. and Katz, I., *Fundamentals of Electric Propulsion: Ion and Hall Thrusters*, JPL, 2008.

[2]Wilbur, P. and Laupa, T., "Plasma contactor design for electrodynamic tether applications," *Advances in space research*, Vol. 8, No. 1, 1988, pp. 221–224.

[3]Gilgenbach, R., Ching, C., Lash, J., and Lindley, R., "Laser diagnostic experiments on KrF laser ablation plasma-plume dynamics relevant to manufacturing applications," *Physics of Plasmas*, Vol. 1, 1994, pp. 1619–1625.

[4]Boyd, I. and Ketsdever, A., "Interactions between spacecraft and thruster plumes." *Journal of Spacecraft and Rockets*, Vol. 38, No. 3, 2001, pp. 380.

[5]Narasimha, R., "Collisionless expansion of gases into vacuum," *Journal of Fluid Mechanics*, Vol. 12, No. 02, Feb. 1962, pp. 294–308.

[6]Mikellides, I. G., Jongeward, G. A., Gardner, B. M., Katz, I., Mandell, M. J., and Davis, V. A., "A Hall-Effect Thruster Plume and Spacecraft Interactions Modeling Package," *27th International Electric Propulsion Conference*, Electric Rocket Propulsion Society, Fairview Park, OH, 2001.

[7]Passaro, A., Vicini, A., and Biagioni, L., "3-D computation of plasma thruster plumes," *40th AIAA/ASME/SAE/ASEE Joint Propulsion Conference & Exhibit*, AIAA, Washington DC, 2004.

[8]Parks, D. and Katz, I., "A preliminary model of ion beam neutralization," *14th International Electric Propulsion Conference*, Electric Rocket Propulsion Society, Fairview Park, OH, 1979.

[9]Ashkenazy, J. and Fruchtman, A., "Plasma plume far field analysis," *27th International Electric Propulsion Conference*, Electric Rocket Propulsion Society, Fairview Park, OH, 2001.

[10]Korsun, A. and Tverdokhlebova, E., "The characteristics of the EP exhaust plume in space," *33rd AIAA/ASME/SAE/ASEE Joint Propulsion Conference & Exhibit*, AIAA, Washington DC, 1997.

[11]Korsun, A., Gabdullin, F., Tverdokhlebova, E., and Borisov, B., "Comparison between Plasma Plume Theoretical Models and Experimental Data," *26th International Electric Propulsion Conference*, Electric Rocket Propulsion Society, Fairview Park, OH, 1999.

[12]Azziz, Y., *Experimental and Theoretical Characterization of a Hall Thruster Plume*, Ph.D. thesis, Massachusetts Institute of Technology, 2007.

[13]Bombardelli, C. and Peláez, J., "Ion Beam Shepherd for Contactless Space Debris Removal," *Journal of Guidance, Control, and Dynamics*, Vol. 34, No. 3, May 2011, pp. 916–920.

[14]Bombardelli, C., Urrutxua, H., Merino, M., Ahedo, E., Pelaez, J., and Olympio, J., "Dynamics of Ion-beam-propelled space debris," *22nd International Symposium on Space Flight Dynamics*, 2011.

[15]Merino, M., Ahedo, E., Bombardelli, C., Urrutxua, H., Pelaez, J., and Summerer, L., "Space Debris Removal with an Ion

Beam Shepherd Satellite: target-plasma interaction," *47th AIAA/ASME/SAE/ASEE Joint Propulsion Conference & Exhibit*, AIAA, Washington DC, 2011.

[16]Merino, M., Ahedo, E., Bombardelli, C., Urrutxua, H., and Pelaez, J., "Ion Beam Shepherd Satellite for Space Debris Removal," *Proceedings of EUCASS 2011, 4-8 July 2011, Saint Petersburg, Russia*, paper 263, 2011.

[17]Liou, J. and Johnson, N., "A sensitivity study of the effectiveness of active debris removal in LEO," *Acta Astronautica*, Vol. 64, No. 2-3, 2009, pp. 236–243.

[18]Aston, G., Kaufman, H., and Wilbur, P., "Ion beam divergence characteristics of two-grid accelerator systems," *AIAA Journal*, Vol. 16, 1978, pp. 516–524.

[19]Nakles, M. R., Brieda, L., Garrett, D. R., Hargus, W. A. J., and Spicer, R. L., "Experimental and Numerical Examination of the BHT-200 Hall Thruster Plume," *43rd AIAA/ASME/SAE/ASEE Joint Propulsion Conference & Exhibit*, AIAA, Washington DC, 2007.

[20]Boyd, I. and Yim, J., "Modeling of the near field plume of a Hall thruster," *Journal of applied physics*, Vol. 95, 2004, pp. 4575.

[21]Boyd, I. and Dressler, R., "Far field modeling of the plasma plume of a Hall thruster," *Journal of applied physics*, Vol. 92, 2002, pp. 1764.

[22]Haas, J. M. and Gallimore, A. D., "An Investigation of Internal Ion Number Density and Electron Temperature Profiles in a Laboratory-Model Hall Thruster," *36th AIAA/ASME/SAE/ASEE Joint Propulsion Conference & Exhibit*, AIAA, Washington DC, 2000.

[23]Martinez-Sanchez, M. and Pollard, J. E., "Spacecraft Electric Propulsion - An Overview," *Journal of Propulsion and Power*, Vol. 14, No. 5, Sept. 1998, pp. 688–699.

[24]Ahedo, E. and Merino, M., "Two-dimensional supersonic plasma acceleration in a magnetic nozzle," *Physics of Plasmas*, Vol. 17, 2010, pp. 073501.

[25]Roberson, B. R., Winglee, R., and Prager, J., "Enhanced diamagnetic perturbations and electric currents observed downstream of the high power helicon," *Physics of Plasmas*, Vol. 18, No. 5, 2011, pp. 053505.

[26]Korsun, A., Tverdokhlebova, E., and Gabdullin, F., "The Earth's Magnetic Field Effect upon Plasma Plume Expansion," *25th International Electric Propulsion Conference*, Electric Rocket Propulsion Society, Fairview Park, OH, 1997.